AIAA-98-4021

RESULTS OF A 24-INCH HYBRID MOTOR PERFORMANCE UNCERTAINTY ANALYSIS

Joseph D. Sims
Lockheed Martin Astronautics
Huntsville, Alabama

Hugh W. Coleman
Propulsion Research Center
Department of Mechanical and Aerospace Engineering
University of Alabama in Huntsville
Huntsville, Alabama

34th AIAA/ASME/SAE/ASEE
Joint Propulsion Conference and Exhibit
July 12-15, 1998 / Cleveland, Ohio

RESULTS OF A 24-INCH HYBRID MOTOR UNCERTAINTY ANALYSIS

Joseph D. Sims*
Lockheed Martin Astronautics - Huntsville Operations
Huntsville, AL 35806

Hugh W. Coleman†
Propulsion Research Center
Department of Mechanical and Aerospace Engineering
University of Alabama in Huntsville
Huntsville, AL 35899

Abstract

The subscale (11- and 24-inch) hybrid motors at the Marshall Space Flight Center (MSFC) have been used as versatile and cost effective testbeds for developing new technology. Comparisons between motor configurations, ignition systems, feed systems, fuel formulations, and nozzle materials have been carried out without detailed consideration as to how "good" the motor performance data were. For the 250,000 lb_f-thrust motor developed by the Hybrid Propulsion Demonstration Program consortium, this shortcoming is particularly risky because motor performance will likely be used as part of a set of downselect criteria to choose between competing ignition and feed systems under development.

This analysis directly addresses that shortcoming by applying uncertainty analysis techniques to the experimental determination of the characteristic velocity, theoretical characteristic velocity, and characteristic velocity efficiency for a 24-inch motor firing. With the adoption of fuel-lined headends, flow restrictors, and aft mixing chambers, state of the art 24-inch hybrid motors have become very efficient. However, impossibly high combustion efficiencies (some computed as high as 108%) have been measured in some tests with 11-inch motors. This analysis has given new insight into explaining how these efficiencies were measured to be so high, and into which experimental measurements contribute the most to the overall uncertainty.

Nomenclature

English

a: Initial throat diameter for erosion model
A^*: Nozzle throat area (in^2)
b: Fitting constant for erosion model
B_i: Bias uncertainty
Bi: Biot number
C*: Characteristic velocity (ft/sec)
C_d: Discharge coefficient
D: Diameter (in)
DRE: Data reduction equation
GOX: Gaseous oxygen
GUI: Graphical user interface
h: Perturbation magnitude
h_g: Hot gas-side convective heat transfer coefficient
HPDP: Hybrid Propulsion Demonstration Program
I_{sp}: Sea-level specific impulse (lbf-sec/lbm)
I_{vac}: Vacuum specific impulse (lbf-sec/lbm)
JIRAD: Joint Independent Research and Development
k: Thermal conductivity (BTU/in-sec-°R)
LOX: Liquid oxygen
LSSRCS: Large Subscale Solid Rocket Motor Combustion Simulator
M: Mass (lbm)
$\dot{m}$: Mass flow rate (lbm/sec)
Nu_D: Nusselt number based upon diameter
ODE: One-dimensional equilibrium
O/F: Oxidizer-to-fuel ratio
P: Pressure (lbf/in^2)
Pr: Prandtl number
P_i: Precision uncertainty
r: Experimental result
Re_D: Reynolds number based upon diameter
SHUE: Software for Hybrid Uncertainty Estimation
SLOC: Source lines of code
t_{burn}: Motor burn time
TEA/TEB: Pyrophoric mixture of triethylaluminum and triethylboride

---

* Propulsion Engineer, Advanced Space Systems, Member AIAA
† Eminent Scholar in Propulsion and Professor, Associate Fellow AIAA

UPC: Uncertainty percent contribution
U_i: Experimental uncertainty
X_i: Primitive measured variable

Greek symbols

α: Coefficient of thermal expansion (1/°R)
ΔT: Temperature difference (°R)
ϕ: Sum of O, O_2 mass fractions in exhaust species
γ: Ratio of specific heats
η_{c^*}: Combustion efficiency
μ: Viscosity (lbm/in-sec)
ρ: Density (lbm/ft^3)

Subscripts and Superscripts

*: Nozzle Throat
Vap: Vapor
0: Chamber condition

Introduction

Lockheed Martin Astronautics' (as the former General Dynamics, then Martin Marietta, before merging to form the current Corporation) involvement with hybrid propulsion development at the Marshall Space Flight Center dates back to 1990, with the formulation and execution of the JIRAD program.

The successful JIRAD program effort was followed in 1992 by the LSSRCS program, a concept that used subscale hybrid motors to simulate the combustion process and exhaust species of a solid rocket motor. Numerous test series were completed that validated this cost effective evaluation process. LMA also supported the HPTLVB program, which started in 1993.

Several hybrid propulsion development programs were integrated in 1994 to form a single, focused effort to develop and test a series of 250,000-pound thrust hybrid motors (250K configuration).

Common to all these programs are three subscale motors at the NASA Marshall Space Flight Center MSFC). Two eleven-inch diameter motor configurations (11" case O.D.) are used, one for GOX and the other for LOX. A twenty four-inch configuration (24" case O.D.) that exclusively uses LOX is also available. The subscale motor configurations have matured throughout the different programs, but all currently use a headend vaporization chamber (lined with either fuel or silica phenolic) and an aft end mixing chamber (similarly lined with fuel or silica phenolic, and in the 11-inch GOX motor, a silica phenolic baffle is also inserted) to enhance combustion efficiency and stability. This pre- and post-chamber configuration has also carried over into the 250K motor.

Another common theme among all the programs, including HPDP, is that no detailed analysis has been done to address measurement uncertainties. The fundamental question that uncertainty analysis attempts to answer is, "How good are the data and the results calculated from them?" The actual process is straightforward, but the final product requires care to be sure all the sources of uncertainty have been accounted for.

In this effort, a FORTRAN 90 computer code was written to calculate uncertainties for 28 different experimental results for the four hybrid motors. The code uses standard analysis techniques to estimate partial derivatives and to propagate those derivatives, along with their associated measurement bias and precision limits, into an overall experimental uncertainty. This overall process is demonstrated using hot-fire data from a recent HPDP 24-inch motor test.

Additionally, some recent 11-inch motor test results show impossibly high combustion efficiencies. It is asserted in this paper that these impossible measurements result from conceptual (modeling) biases in the calculation procedures.

Uncertainty Analysis

Only a brief overview of the methodology to obtain uncertainty estimates and how they propagate through a given DRE is given here. The reader is referred to Coleman and Steele[1,2] for a detailed discussion of uncertainty analysis techniques.

The word accuracy is generally used to indicate the relative closeness of agreement between an experimentally determined value of a quantity and its true value. Error is the difference between the experimentally determined value and the truth; therefore, as error decreases, accuracy is said to increase. Only in rare instances is the true value of a quantity known. Thus, it is necessary to estimate error, and that estimate is called an uncertainty, U. Uncertainty estimates are made at some confidence level – a 95% confidence estimate, for example, means that the true value of the quantity is expected to be within the ±U interval about the experimentally determined value 95 times out of 100.

Total error can be considered to be composed of two components: a precision (random)

component, ε, and a bias (systematic) component, β. An error is classified as precision if it contributes to the scatter of the data; otherwise, it is a bias error. As an estimator of β, a systematic uncertainty or bias limit, B, is defined. A 95% confidence estimate is interpreted as the experimenter being 95% confident that the true value of the bias error, if known, would fall within ±B. A useful approach to estimating the magnitude of a bias error is to assume that the bias error for a given case is a single realization drawn from some statistical parent distribution of possible bias errors. As an estimator of the magnitude of the precision errors, a precision uncertainty or precision limit, P, for a single reading is defined. A 95% confidence estimate of P is interpreted to mean that the ±P interval about the single reading of X_i should cover the (biased) parent population mean, μ, 95 times out of 100.

In nearly all experiments, the measured values of different variables are combined using a DRE to form some desired result. A general representation of a DRE is

$$r = r(X_1, X_2, \ldots, X_J) \qquad (1)$$

where r is the experimental result determined from J measured variables X_i. Each of the measured variables contains bias errors and precision errors. These errors in the measured values then propagate through the DRE, thereby generating the bias and precision errors in the experimental result, r.

If the "large sample assumption" is made[2], then the 95% confidence expression for U_r becomes

$$U_r^2 \approx B_r^2 + P_r^2 \qquad (2)$$

where the systematic uncertainty (bias limit) of the result is defined as

$$B_r^2 = \sum_{i=1}^{J} \theta_i^2 B_i^2 + 2\sum_{k=1}^{J-1}\sum_{l=k+1}^{J} \theta_k \theta_l B_{kl} \qquad (3)$$

with the bias limit estimate for each X_i variable as the root sum square combination of its elemental systematic uncertainties

$$B_i = \left[\sum_{j=1}^{M} (B_i)_j^2\right]^{1/2} \qquad (4)$$

and where B_{kl}, the 95% confidence estimate of the covariance appropriate for the bias errors in X_k and X_l, is determined from

$$B_{kl} = \sum_{a=1}^{L} (B_k)_a (B_l)_a \qquad (7)$$

where variables X_k and X_l share L identical error sources. These terms account for correlation between bias errors in different measurements.

For the analysis summarized in this paper, it was assumed that bias uncertainties dominated the overall measurement uncertainty, making precision uncertainties negligible. The only measurements where precision uncertainties are important are for nozzle throat diameter measurements and the fuel weights. As will be discussed, significant non-symmetric erosion typically occurs at the throat region. These random (from a pre-test prediction standpoint) variances in the throat diameter are treated mathematically as precision uncertainty sources, but in reality, are a unique class of bias uncertainty sources termed fossilized biases. This mathematical treatment can be found in any statistics text, but the 95% confidence large sample precision limit is estimated as

$$P_{\bar{X}_i} = 2\frac{\left[\frac{1}{N-1}\sum_{k=1}^{N}\left[(X_i)_k - \overline{X_i}\right]^2\right]^{1/2}}{\sqrt{N}} \qquad (8)$$

Inspection of equation (3) shows a significant effect that correlated bias uncertainties can have. Because of the covariance expression of the latter half of the right hand side, and most especially because the individual partial derivatives are used (as opposed to their squares), the correlated bias terms can either increase the overall uncertainty (if the partials are of the same sign) or decrease the overall uncertainty (if the partials are of opposite sign). This fact plays a distinct role in this analysis.

Performance Calculations

Measured C*

C* is one measure of the energy content in a chemical propellant combination. It is defined as

$$C^* = \frac{P_0 A^*}{\dot{m}} \qquad (9)$$

However, instantaneous fuel flow rates in hybrid rocket motors are currently difficult, if not impossible, to measure with any reasonable certainty. Therefore, fuel usage is measured by weighing the fuel grains (for the 11-inch) or the loaded motor case (for the 24-inch and 250K motors) both pre- and post-test, and calculating an average fuel flow rate. The result is that C* measurements must be based upon expended values for fuel, ignitor and inert propellant and LOX weights, average nozzle throat area, and a total pressure integral. In effect, all the variables are integrated over the motor burn time, resulting in a modified from of (9):

$$C^* = \frac{\overline{A^*}\left[\frac{1}{t_1 - t_0}\int_{t_0}^{t_1} P_0\,dt\right]}{\frac{1}{t_1 - t_0}\left[\int_{t_0}^{t_1} \dot{m}_{LOX}\,dt + \int_{t_0}^{t_1} \dot{m}_{Fuel}\,dt + \int_{t_0}^{t_1} \dot{m}_{N_2}\,dt + \int_{t_0}^{t_1} \dot{m}_{TEA}\,dt\right]} \qquad (10)$$

The denominator of (10) results from accounting for all fluids that are heated and expelled through the motor nozzle. This includes, of course, the main LOX and fuel, but also includes the TEA/TEB ignition fluid and nitrogen purge masses.

It should be noted that the time interval used to calculate each average factors out of equation (10). Additionally, the integrals in (10) are calculated using a trapezoidal rule approximation – except for the fuel total mass, which is calculated by direct fuel weights pre- and post-test. The appendix contains the general DRE used to calculate motor C*.

Nearly all the terms in the DRE shown in the appendix can be broken down into constituent components. For example, A* is the simple average of the pre-and post-fire throat areas. But, to complicate things further, both of the diameters used in the average area calculation are themselves simple averages of four (each) pre- and post-fire measurements (see the equation below).

$$\overline{D_t} = \frac{D_0 + D_{45} + D_{90} + D_{135}}{4} \qquad (11)$$

The ramification of equation (11), explored in greater detail later in this paper, is that the throat area is assumed to change linearly – i.e., the average throat diameter changes as a second-order function of time.

The LOX mass flow rate is metered using a cavitating venturi, which requires the measurement of inlet pressure and temperature. The flow rate was initially calculated using:

$$\dot{m}_{LOX} = \frac{\pi}{4} D_t^2 C_d \sqrt{\rho(P_{Up} - P_{Vap})} \qquad (12)$$

However, a venturi for use in LOX service is typically calibrated in a room-temperature water facility[2]. This means that, due to the cryogenic temperature during motor firing, the actual venturi throat diameter is somewhat smaller – introducing a bias into the LOX flow rate measurements. One involved method for calculating the actual throat area would require the use of a finite element model. An easier method, however, is to simply use the coefficient of thermal expansion and the temperature difference between the calibration facility and the cryogenic feedline to reduce the throat diameter an appropriate amount, resulting in a slightly modified form of (12)

$$\dot{m} = \frac{\pi}{4}\left[(1 + \alpha\Delta T)D_t\right]^2 C_d \sqrt{\rho(P_{Up} - P_{Vap})} \qquad (13)$$

Equation (13) has two terms that are dependent upon the inlet temperature; namely, ρ and P_{Vap}. These two quantities are calculated using GASP[3] and a Wagnerian curvefit[4], respectively.

Two types of ignition sources are used for the subscale motors. The 11-inch GOX motor uses a small GOX-hydrogen torch, and all three LOX motors use TEA/TEB, a pyrophoric fluid. Following a pre-set length of time over which the torch is lit or TEA/TEB is flowing, a gaseous nitrogen purge is started to keep combustion products from flowing back into the ignition feed system. Therefore, (12) is used to calculate TEA/TEB flow rate, with the density modeled as a function of temperature only (a conceptual bias), and with the vapor pressure assumed to be zero[5].

Nitrogen is metered using the same orifice as for the TEA/TEB (or the GOX-hydrogen torch). The equation for sonic gas flow through a sharp-edged orifice is

$$\dot{m}_{N_2} = \frac{\frac{\pi}{4}\sqrt{\left(\frac{2}{\gamma+1}\right)^{\frac{\gamma+1}{\gamma-1}}} C_d D_{Orf}^2 P_{Up}}{\sqrt{RT_{Up}}} \qquad (14)$$

The nitrogen γ is also calculated using GASP.

The fuel integral is a simple weight change calculation based upon average pre- and post-fire weighing:

$$\int_{t_0}^{t_b} \dot{m}_{Fuel} = \overline{M}_{Pre} - \overline{M}_{Post} = \frac{1}{3}\left[\begin{array}{l}\left(M_{Pre_0} + M_{Pre_1} + M_{Pre_2}\right) - \\ \left(M_{Post_1} + M_{Post_2} + M_{Post_3}\right)\end{array}\right] \quad (15)$$

Differentiation of (15) shows clearly that the pre- and post-fire grain weight measurements have derivatives that are of opposite sign. This fact, highlighted in a previous section, helps to reduce the overall measurement uncertainty. The pre- and post-fire measurements have correlated bias uncertainties because the same load cell (or scale, for the lighter motor pieces) is used for both sets of weights. Since a bias uncertainty is systematic, the magnitude of the uncertainty does not change from pre- to post-test weightings. In effect, the bias is "calibrated out," resulting in a more certain weight difference measurement than either individual pre- or post-fire weights.

One additional point that should be noted is that the chamber pressure integral (and resulting average), was originally based upon measurements taken in the headend of the motor. A well-known phenomenon exists in solid and hybrid rocket motors, however, such that there can be a significant pressure drop down the length of the motor that is a complex function of chamber conditions and flow rate. With the addition of a mixing chamber aft of the fuel grain in hybrid motors (which promotes combustion product stagnation due to a diffuser-like effect and amplifies the pressure drop), it was felt that using headend pressure measurements contributed another conceptual bias to the performance calculations.

Overall, the DRE for measured C* becomes a complicated amalgam of expressions (see appendix) that defies closed form partial derivative calculations.

Theoretical C*

Estimating the uncertainties associated with a theoretical model is a relatively new addition to the uncertainty analysis arena. Coleman and Stern[7] have investigated using uncertainty techniques to validate a CFD code in which the validation level is set by the combination of the uncertainties in the experimental data and the portion of the uncertainties in the code that can be estimated. Brown and Coleman[8] also investigated how measurement uncertainties affected the modeling of the SSME power balance. A similar process to that used in Coleman and Stern was used for the work reported in this paper, though no attempt was made to estimate the uncertainties in the theoretical calculations themselves. The uncertainty in the theoretical C*, then, results directly from uncertainties in the input data.

Historically, theoretical C* was calculated by interpolating tabulated values that resulted from thermochemistry runs completed by a consortium member. The values were tabulated as a function of O/F and chamber pressure. However, the values did not account for the TEA/TEB, the GOX-hydrogen torch gases, the silica phenolic from the aft mixing chamber and the baffle (in the 11-inch GOX motor) or the nitrogen purge. It was felt all these fluids contributed to the measured C* pressure integral and to the theoretical calculations, and that not accounting for them introduced additional biases into the experimental results. Therefore, this analysis used the latest release of the classic NASA-Lewis ODE module written by Gordon and McBride called CEA[5], along with a complete input of all the propellants expended during a test.

Aft pressure measurements were also used for input to CEA. Other inputs include motor propellant formulation -- calculated during mixing and casting operations -- and O/F -- calculated using total expended propellants via direct weight measurements or integrated mass flow rates.

Since a computer code is now used to calculate the theoretical C*, closed form solution for partial derivatives is rendered impossible. Therefore, they, too, were estimated numerically by perturbing individual measurements which affected the CEA input data.

C* Efficiency

C* efficiency is a measure of how much energy is released by combustion -- as gauged by the pressure generated -- compared to the theoretical chemical potential energy stored in the propellant(s). A simple equation for combustion efficiency is

$$\eta_{C^*} = \frac{C^*_{Measured}}{C^*_{ODE}} \quad (16)$$

Since both the denominator and the numerator are themselves functions of numerous

primitive variables and inputs, equation (16) is meant only to convey the notion of combustion efficiency.

Computer Code

User Interface

Due to the requirement to integrate mass flow rates and the fact that closed form solutions for partial derivatives were rendered impossible, a computer program was written for this analysis. It is a Windows™-based, FORTRAN 90 routine that incorporates GASP and CEA. A Visual FORTRAN™ GUI' was written to make the code as simple to use as possible. Figure 1 shows the opening screen for SHUE.

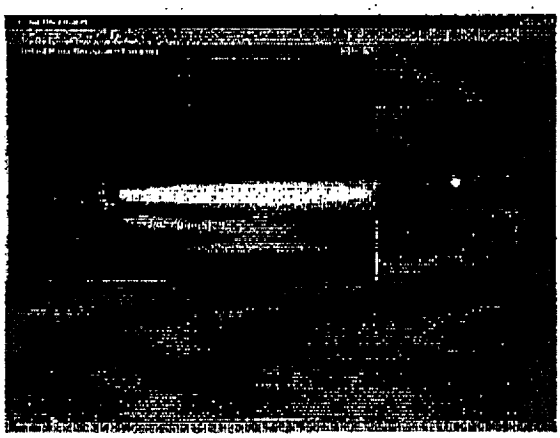

Fig. 1: SHUE opening screen.

SHUE will be capable of performing 28 separate uncertainty analyses, ranging from mass flow rate and total impulse uncertainties to C*, I_{sp} and I_{vac} (measured, theoretical and efficiency) uncertainties. Currently, all but the I_{sp} and I_{vac} analyses are complete and validated. To date, there are approximately 25,000 SLOC, of which 8,000 are from GASP and CEA. Once completed, it is estimated SHUE will contain more than 30,000 SLOC.

The user is required to input which motor is being analyzed, which fuel formulation was used, and a test name, as well as pre- and post-test measurements for fuel grain weights and nozzle dimensions. Additional input includes fluid meter parameters, elemental bias limit estimates, and the data-sampling rate. A typical input dialog appears in Figure 2.

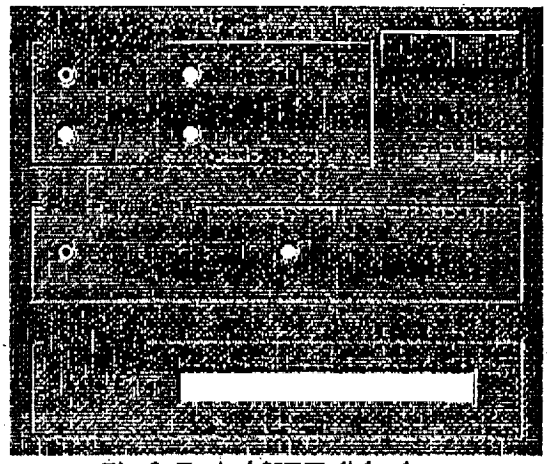

Fig. 2: Typical SHUE dialog box.

Once all of the required information is provided, the user selects any or all of the analyses that are required to be performed. This is selected through the drop-down menus at the top of the program window, an example of which is shown in Figure 3.

Fig. 3: Selection of an uncertainty analysis.

After selecting which analyses to perform, the user then opens the data file for the motor test and selects "Go!" under the "File" menu. Depending upon the analysis, the user may be required to input start- and stop-times for the limits of integration. Run-times vary from a few seconds to three hours. Analysis results are currently output to an ASCII text file.

Algorithm Description

The repetitive algorithm used for SHUE is straightforward, but because of the shear number of calculations, the algorithm is quite intricate. After the

user inputs the required data and times, the code loops through every measurement (pressures, temperatures, et cetera) to calculate a nominal value of the experimental result. Calculations for nozzle and weight measurements are completed during user input, and the integrals are calculated using the trapezoidal rule. Other, more sophisticated schemes for numerical integration were initially considered, but were abandoned because results for the trapezoidal rule were nearly identical and required less CPU time.

Once the nominal result is calculated, the partial derivatives are estimated by singly perturbing every measurement used in the nominal calculation by 0.5% -- hence the name "jitter" routine – and using equation (3). It should be noted that perturbing a single variable in an integral means that a complete integral is required with each pass through the loop. In other words, if there are 5000 pressure data points, a single point is perturbed and a new integral with that single perturbed variable (along with the other 4999 nominal data points) is calculated. This fact required that the code be written using REAL*8 variables in order to calculate the derivatives with sufficient accuracy. This jitter process was repeated for every variable that affected the experimental result. For example, there are 25 types of measurements which affect motor C* efficiency. Of those 25 types, 9 involve recalculating integrals for each of the multiple measurements taken in that type (venturi inlet pressure, for example), resulting in approximately 12,300 partial derivatives for a typical 20-second test.

Once each partial derivative is calculated the code passes control to the uncertainty propagation subroutine, where the partial derivatives are combined with the uncertainty estimates. Another parameter is also calculated in this portion of the code: the UPC.

Most simply, the UPC allows the ranking of the most significant uncertainty contributor(s) by tabulating what percent of the overall uncertainty-squared each type of measurement contributes. Equation (17) shows how the UPC is calculated for each variable:

$$UPC = \frac{\left(\frac{\partial r}{\partial X_i} U_{x_i}\right)^2}{U_r^2} * 100 \qquad (17)$$

Results and Discussion

24-Inch Motor

In order initiate validation of SHUE, data from a 24-inch test (HP24-5030) was used for this analysis, as that test was a close analog to the upcoming 250K motor tests. Once SHUE is complete and validated, the HP24–5030 test data will be scaled to match expected conditions for the 250K test firing. The scaling will be done in order to get a pre-test uncertainty prediction, so that an understanding can be derived as to which measurements are most important for reducing the uncertainty in the full scale motor tests.

There are 23 variables or measurements that are required to calculate C* (measured, theoretical, and efficiency). Factory specifications were used for estimating bias limits for pressure transducers, thermocouples, and load cells. Estimates for the venturi and orifice calibration biases were assumed based upon the results of an unpublished calibration analysis for the 250K motor venturi completed by engineers at MSFC. LOX ρ and nitrogen γ biases were taken from the GASP user's manual, as stated in [2]. The LOX vapor pressure bias estimate was taken as the largest reported error estimate in [4]. Finally, weight percent bias estimates for each constituent in the fuel formulation was based upon a conservative estimate (i.e., larger than is probable) of the bias in the scale used at the casting facility divided by each constituent's total weight per mix.

It should be noted that there are only three measurements that have the potential for significant uncertainties introduced from precision sources: the nozzle throat diameter measurements, the fuel grain weights, and the headend weights. The nozzle throat measurements will be discussed separately, but typically, asymmetric erosion occurs during the motor firing. These asymmetries are treated like precision errors and combined with the bias limit for the calipers used, by using a root-sum-square method. Similar procedures are used for the grain and headend weights, though the precision contribution is small in both cases. Table 1 summarizes each measurement along with its nominal value and bias limit.

Parameter	Nominal Value	Bias Limit
$P_{Chamber}$	580 psia	5 psi
$P_{LOX\ Inlet}$	1500 psia	7 psi
$T_{LOX\ Inlet}$	-268 °F	3 °F
$P_{Nitrogen\ Inlet}$	1500 psia	5 psi
$T_{Nitrogen\ Inlet}$	71 °F	3 °F
$P_{LOX\ Vapor}$	65.5 psi	0.1% Reading
ρ_{LOX}	68 lbm/ft³	0.25% Reading
ρ_{TEA}	44 lbm/ft³	10% Reading
$\gamma_{Nitrogen}$	1.4447	0.5% Reading
LOX Venturi C_d	0.9622	0.019 (2%)
LOX Venturi α	9.6×10^{-6}/°F	10% Reading
LOX Venturi $T_{Calibration}$	70 °F	5 °F
N_2 Orifice C_d	0.80	0.016 (2%)
N_2 Orifice Diameter	0.09 in.	0.005 in.
Grain Weight Loss	322 lbm	25 lbm[†]
Headend Weight Loss	28.4 lbm	0.005 lbm[§]
D*	4.6 in.	0.010 in.
Escorez wt%[‡]	N/A	1×10^{-1} %
R-45 wt%	N/A	2×10^{-4} %
DDI wt%	N/A	6×10^{-4} %
Voranol wt%	N/A	1×10^{-3} %
Agerite White wt%	N/A	1×10^{-3} %
Carbon Black wt%	N/A	3×10^{-3} %

Table 1: Bias limits for each experimental parameter.

In general, the C* measurements are fairly good – C* efficiency had a ± 2% uncertainty band. Table 2 summarizes the results of the analysis, and compares the old calculation method results with the new method proposed in this paper. The comparison shows that the changes in procedure affects the results at a magnitude lower than the overall uncertainty – i.e., the changes, for all practical purposes, cannot be seen for lack of measurement resolution. However, the "lessons learned" in this process have more significant ramifications for the 11-inch GOX motor.

	Old Value	New Value	Uncertainty
$C^*_{Measured}$	5753 ft/sec	5775 ft/sec	113 ft/sec
C^*_{Theory}	5769 ft/sec	5772 ft/sec	14 ft/sec
η_{C^*}	99.7%	100%	2%

Table 2: Overall uncertainty analysis results.

The detailed breakdown of uncertainty contributions is interesting, and is probably more informative. Tables 3 through 5 summarize UPC values, with uncorrelated and correlated UPC components reported for all three experimental results. Note that six measurements ($P_{LOX\ Vapor}$, $P_{Nitrogen\ Inlet}$, $T_{Nitrogen\ Inlet}$, LOX Venturi α, $\gamma_{Nitrogen}$, ρ_{TEA}, and N_2 Orifice C_d) do not appear in the following three tables. They each contribute less than 0.01% to the measurement uncertainty for the three experimental results.

Parameter	UPC Component(s)	Resultant Measurement UPC
LOX Venturi C_d	51.04%	51.04%
LOX Venturi $T_{Calibration}$	2.12%	2.12%
Uncorrelated $P_{Chamber}$	0.01%	
Correlated $P_{Chamber}$	19.07%	19.08%
Uncorrelated $P_{LOX\ Inlet}$	0.00%	
Correlated $P_{LOX\ Inlet}$	0.86%	0.86%
Uncorrelated $T_{LOX\ Inlet}$	0.01%	
Correlated $T_{LOX\ Inlet}$	5.44%	5.45%
Uncorrelated ρ_{LOX}	0.00%	
Correlated ρ_{LOX}	0.20%	0.20%
Uncorrelated N_2 Orifice Diameter	0.06%	
Correlated N_2 Orifice Diameter	0.07%	0.13%
Uncorrelated Pre-Fire D*	0.20%	
Uncorrelated Post-Fire D*	4.42%	
Correlated Pre-Fire D*	0.60%	
Correlated Post-Fire D*	13.27%	
Correlated Pre- and Post-Fire D*	2.32%	20.82%
Uncorrelated Pre-Fire Headend Weight	0.00%	
Uncorrelated Post-Fire Headend Weight	0.00%	
Correlated Pre-Fire Headend Weight	0.00%	
Correlated Post-Fire Headend Weight	0.00%	
Correlated Pre- and Post-Fire Headend Weight	-0.00%	0.00%
Uncorrelated Pre-Fire Center Segment Weight	36.71%	
Uncorrelated Post-Fire Center Segment Weight	37.73%	
Correlated Pre-Fire Center Segment Weight	73.42%	
Correlated Post-Fire Center Segment Weight	75.47%	
Correlated Pre- and Post-Fire Center Segment Weight	-223.10%	0.24%

Table 3: Detailed UPC values for $C^*_{Measured}$.

[†] These bias limits apply to each individual pre- and post-fire measurement and *not* to the overall weight difference (see Uncertainty Analysis for explanation).
[‡] Due to ITAR restrictions, these nominal values cannot be reported.

Parameter	UPC Component(s)	Resultant Measurement UPC
LOX Venturi C_d	72.68%	72.68%
LOX Venturi $T_{Calibration}$	3.00%	3.00%
Uncorrelated $P_{Chamber}$	0.00%	
Correlated $P_{Chamber}$	0.19%	0.19%
Uncorrelated $P_{LOX\ Inlet}$	0.00%	
Correlated $P_{LOX\ Inlet}$	2.08%	2.08%
Uncorrelated $T_{LOX\ Inlet}$	0.00%	
Correlated $T_{LOX\ Inlet}$	5.91%	5.91%
Uncorrelated ρ_{LOX}	0.00%	
Correlated ρ_{LOX}	0.54%	0.54%
Uncorrelated N_2 Orifice Diameter	0.62%	
Correlated N_2 Orifice Diameter	-0.54%	0.09%
Uncorrelated Fuel Constituent Weight %	1.08%	
Correlated Fuel Constituent Weight %	0.22%	1.29%
Uncorrelated Pre-Fire Headend Weight	0.00%	
Uncorrelated Post-Fire Headend Weight	0.00%	
Correlated Pre-Fire Headend Weight	0.00%	
Correlated Post-Fire Headend Weight	0.00%	
Correlated Pre- and Post-Fire Headend Weight	-0.00%	0.00%
Uncorrelated Pre-Fire Center Segment Weight	274.84%	
Uncorrelated Post-Fire Center Segment Weight	345.73%	
Correlated Pre-Fire Center Segment Weight	549.68%	
Correlated Post-Fire Center Segment Weight	691.46%	
Correlated Pre- and Post-Fire Center Segment Weight	-1847.72%	13.99%

Table 4: Detailed UPC/UMF values for C^*_{Theory}

It should be stressed that for all three cases, the most significant contributor to the overall experimental uncertainty is the LOX venturi C_d. In addition, the fuel grain and headend weight measurements are negligible contributors to the overall uncertainty. Some discussion provides some insight as to why those measurements once appeared to contribute significantly.

Parameter	UPC Component(s)	Resultant Measurement UPC
LOX Venturi C_d	42.90%	42.90%
LOX Venturi $T_{Calibration}$	1.84%	1.84%
Uncorrelated $P_{Chamber}$	0.01%	
Correlated $P_{Chamber}$	23.40%	23.41%
Uncorrelated $P_{LOX\ Inlet}$	0.00%	
Correlated $P_{LOX\ Inlet}$	0.67%	0.67%
Uncorrelated $T_{LOX\ Inlet}$	0.00%	
Correlated $T_{LOX\ Inlet}$	4.92%	4.93%
Uncorrelated ρ_{LOX}	0.00%	
Correlated ρ_{LOX}	0.15%	0.15%
Uncorrelated N_2 Orifice Diameter	0.10%	
Correlated N_2 Orifice Diameter	0.00%	0.10%
Uncorrelated Fuel Constituent Weight %	0.02%	
Correlated Fuel Constituent Weight %	0.00%	0.02%
Uncorrelated Pre-Fire D*	0.24%	
Uncorrelated Post-Fire D*	5.29%	
Correlated Pre-Fire D*	0.72%	
Correlated Post-Fire D*	15.88%	
Correlated Pre- and Post-Fire D*	2.77%	24.91%
Uncorrelated Pre-Fire Headend Weight	0.00%	
Uncorrelated Post-Fire Headend Weight	0.00%	
Correlated Pre-Fire Headend Weight	0.00%	
Correlated Post-Fire Headend Weight	0.00%	
Correlated Pre- and Post-Fire Headend Weight	-0.00%	0.00%
Uncorrelated Pre-Fire Center Segment Weight	78.90%	
Uncorrelated Post-Fire Center Segment Weight	86.43%	
Correlated Pre-Fire Center Segment Weight	157.79%	
Correlated Post-Fire Center Segment Weight	172.86%	
Correlated Pre- and Post-Fire Center Segment Weight	-494.98%	1.00%

Table 5: Detailed UPC/UMF values for η_{c^*}

Inspection of the three tables shows a significant sensitivity to the overall result for *either*

pre- or post-fire weights – which seems intuitive. However, as explained in the Uncertainty Analysis section, the partial derivatives for the weight measurements are of opposite sign, resulting in the small UPC for all three experimental results. This is most dramatically evidenced by the enormous correlated bias contribution made by the center segment weights. In effect, the weight difference can be measured to a much higher degree of accuracy than either individual pre- or post-fire weights.

Another significant bias contributor is the nozzle throat diameter measurements. The individual throat measurements are quite good: the caliper bias used for this analysis was conservatively estimated to be 0.010" – of which 0.001" comes from the caliper calibration, and the order of magnitude increase comes from estimated errors in being able to consistently measure the same point on the throat (depth, angle, etc.). The majority of that large overall contribution comes from the post-fire measurements.

This is based upon the fact that nozzles with a significant erosion rate see a measurable asymmetric erosion pattern. Table 6 summarizes the pre- and post-fire measurements for the nozzle used in HP24-5030. As can be seen, there is significant variation in the measured diameter.

Measurement Clocking	Pre-Fire Diameter (in.)	Post-Fire Diameter (in.)
0° - 180 °	3.706	5.375
45° - 225 °	3.706	5.278
90° - 270 °	3.706	5.269
135° - 315 °	3.706	5.386
Average	3.706	5.327

Table 6: Nozzle throat measurements for HP24-5030.

This diameter variation, in reality, represents a source of precision uncertainty. That is, until more quantitative data exist as to actual flowfield conditions the variance can be considered a random effect. The most common way to account for precision uncertainties is by standard statistical analysis, which was the method used for this analysis. While these aren't strictly *measurement* uncertainties, they do fall into the conceptual bias category. This is because the C* equation assumes a *circular* throat area; in effect, forcing the calculated area to be circular despite the evidence to the contrary. Further, because the erosion patterns are asymmetric, the resulting average post-fire diameter will be completely dependent upon where the measurements are taken. For example, if the throat were inadvertently clocked by 30° and measured again, the average would be quite different. Therefore, the best way to estimate that bias uncertainty is by calculating the precision index, $P_{\bar{x}}$, (based upon the precision index of the mean), and treating that index as a fossilized bias.

The overall post-fire throat diameter bias, then, was nearly an order of magnitude higher than the 0.010" bias from the actual measurement instrument: it was calculated as 0.099". The authors assert that doubling or tripling the number of post-fire measurements would reduce the effects of this conceptual bias to a more acceptable level.

11-Inch Motor Considerations

Another issue that is related to nozzle throat erosion has stemmed from the results of some recent 11-inch GOX motor firings. These motors appear to have impossibly high combustion efficiencies – 107.4% for HP11-4010, for example. As mentioned previously, using the aft pressure trace, accounting for the silica phenolic weight, and using CEA to calculate the theoretical C* reduces the efficiency to 102.1%. This value is only 2% higher than the theoretical maximum, within the uncertainty band for the measured C* calculation. However, the 11-inch GOX motors consistently run higher than 100% efficiencies, which suggests that there is a bias that has not been addressed. Some have suggested that perhaps the average throat area calculation needs adjusting for the GOX motors. In fact, the difficulty with the throat area calculation, historically, is the reason that some propulsion specialists prefer I_{sp} efficiency measurements[10].

The simplest change one could consider making to the average throat area calculation is to assume that throat *diameter* (not area) is a linear function of time. That is, assume the throat diameter increases at a constant, time-averaged rate. Doing so reduces the efficiency for HP11-4010 to 99.2%, a slightly more believable level of performance. However, it is difficult, considering the highly complex (and mostly unexplored) heat transfer and erosion characteristics of hybrid motor nozzle throats, to assume a simple, linear phenomenon is controlling erosion.

A different method to consider appears to be closer to the true nozzle response. A theory was postulated by one consortium member that assumes for a small, but measurable time, the nozzle wall acts much like a heat sink while it reaches the temperature required to ablate the graphite throat[11] – suggesting some parabolic or exponential function. To test this

hypothesis, throat diameter histories for 3 recent 11-inch tests were curve-fit using an exponential function of the form

$$d^* = a\exp\left(\frac{t_{burn}}{b}\right) \qquad (18)$$

where a is equal to the initial throat diameter and b is a constant. Parameters a and t_{burn} have direct physical significance, so to be a meaningful model, b should also have some physical significance. The actual throat conditions are difficult to measure, so four non-dimensional parameters were chosen to describe them, in anticipation that the parameter b would be a function of these parameters.

First, to account for the fluid dynamic effects that contribute to mechanical erosive effects, the Reynolds number based upon diameter (Re_D) was chosen. Second, to account for the heat transfer effects that contribute both to mechanical and chemical erosive effects, both the Nusselt number (where h_g – based upon *initial* throat diameter -- was estimated using the Bartz equation[12]) and the Prandtl number were chosen. And finally, because excess oxidizing species can enhance throat erosion due to the formation of CO and CO_2 through scavenging of the graphite, the sum of the mass fractions of O and O_2 in the exhaust species was chosen. In order to factor out the dependence of Re_D and Nu_D upon the throat diameter, the product of those two parameters was used (see the equation below). Additionally, all theoretical parameters (except the film coefficient, as described above) were taken from CEA output.

$$Nu\,\mathrm{Re} = \frac{h_g D}{k}\frac{4\dot{m}}{\pi\mu D} = \frac{4h_g\dot{m}}{\pi\mu} \qquad (19)$$

Results of curvefits between b and the non-dimensional parameters show a remarkable relationship. That final curvefit is shown in Equation (20).

$$b = \phi^{0.4382}\left(Nu\,\mathrm{Re}\right)^{-0.4171}\mathrm{Pr}^{-19.575} \qquad (20)$$

To generate confidence in the curvefit, test data from the JIRAD program were used to compare curvefit predictions from Eq. (20) with curvefits of throat diameter data using Eq. (18). Those results, summarized in Table 7, confirm that for this motor configuration, the constant b does have physical significance to actual motor conditions. This realization lends credibility to the claim that the throat erodes as an exponential function of time. It should be stressed that equation (20) is not yet capable of predicting throat erosion, as seen by the relatively high relative error for JIRAD 9. Additionally, another result for a test with an O/F near stoichiometric conditions showed virtually no agreement. This effort was only to deduce whether (18) was an adequate engineering model, not a prediction tool.

Motor	b (Eq. 22)	b (Eq. 24)	% Error
JIRAD 4	47.7	49.7	4%
JIRAD 9	34.6	46.7	35%
JIRAD 16	32.3	28.0	13%

Table 7: Comparison of erosion models.

As a final check, the Biot number (B_i, the ratio between the thermal resistances to convection and conduction) for HP11-4010 was calculated to be ~700, which shows that the 1-D throat thermal gradient is very steep, further indicating the throat indeed acts as a heat sink.

Table 8 shows how significantly the choice of models affects η_{c^*}.

Linear Area Change	Linear Diameter Change	Exponential Diameter Change
102.1%	99.2%	97.3%

Table 8: η_{c^*} using the three erosion models.

These results suggest a need to begin using (18) for calculating average throat area. The erosion data have more than a coincidental relationship to the major non-dimensional parameters that govern heat transfer. Additionally, it has been suggested that there is an unaccounted-for bias that most likely comes from throat area calculations. Therefore, the authors suggest using Equation (18) for all throat area calculations for the 11-inch motor.

How this applies to the 24-inch and 250K motors is unclear, but will be investigated in the near future. A 3-D carbon cloth/phenolic throat is typically used for those motors, so its through-ply thermal conductivity will vary from that assumed for the graphite throat. So, while the reliance on non-dimensional heat transfer and flow parameters will likely result, it is doubtful equation (20) is directly applicable.

Conclusions

Measurement uncertainty was estimated for three performance parameters used in rocket propulsion testing. Results showed that measured C*, theoretical C*, and C* efficiency uncertainties are most sensitive to LOX mass flow rate, chamber pressure, and nozzle throat diameter. It was also shown that fuel grain weight measurements are negligible contributors to these uncertainties. Additionally, increasing the number of post-fire nozzle throat measurements would reduce experimental uncertainties, which is a result of the significant asymmetric erosion typically found.

Throat erosion models and throat area calculations were investigated as a possible source of conceptual biases which result in impossibly high C* efficiencies. The investigation showed that the nozzle throat in a hybrid motor likely erodes as an exponential function of time, not a linear function of time as previously assumed. The erosion model was compared to a simple theoretical model consisting of four major heat transfer and fluid flow parameters, and showed good agreement. These results indicate that that an exponential-type throat erosion model is fully based in physical parameters that govern heat transfer.

Future work on SHUE will continue, with I_{sp} and I_{Vac} performance measurement capability added. In addition, new throat erosion models will be incorporated, as well as improved bias source estimates and 250K motor configuration fidelity. Uncertainty estimates based upon expected operation for the 250K motor will also be generated. Finally, throat erosion modeling will continue, and will incorporate the more extensive database of 24-inch motor test data.

Acknowledgements

The authors would like to acknowledge the efforts of NASA, DARPA, and the involved industry partners in the organization and execution of the HPDP. We would also like to thank Lockheed Martin Astronautics, in particular, for sponsoring this research.

References

[1] Coleman, H.W. and Steele, G.W., *Experimentation and Uncertainty Analysis for Engineers*, John Wiley & Sons, New York, 1989.

[2] Coleman, H.W. and Steele, W.G., "Engineering Application of Experimental Uncertainty Analysis," *AIAA Journal*, Vol. 33, No. 10, 1995.

[3] Coleman, H.W., and Brown, K.K., "Impact of Uncertainty on Modeling and Testing," Final Report for Contract No. NAS8-38609, NASA MSFC, April 1995.

[4] Hendricks, R.C., Baron, A.K., and Peller, I.C., "GASP – A Computer Code for Calculating the Thermodynamic and Transport Properties for Ten Fluids: Parahydrogen, Helium, Neon, Methane, Nitrogen, Carbon Monoxide, Oxygen, Fluorine, Argon, and Carbon Dioxide," NASA TN D-7808, February 1975.

[5] Wagner, W., Ewers, J., and Pentermann, W, "New Vapour-Pressure Measurements and a New Rational Vapour-Pressure Equation for Oxygen," J. Chem. Thermodynamics, Vol. 8, 1976.

[6] Lide, D.R., Editor-in-Chief, *CRC Handbook of Chemistry and Physics, 77th Ed.*, CRC Press, New York, 1996.

[7] Coleman, H.W. and Stern, F., "Uncertainties and CFD Code Validation," J. Fl. Engineering, Vol. 119, 1997.

[8] Brown, K.K. and Coleman, H.W., "Determination of Uncertainties for the New SSME Model," Final Report for Contract No. NAS8-38609, May 1996.

[9] McBride, B.J. and Gordon, S., "Computer Program for Calculation of Complex Chemical Equilibrium Compositions and Applications," Vol. II, User's Manual and Program Description, NASA Lewis Research Center, June 1996.

[10] *DigitalVisual FORTRAN Language Reference Manual*, Digital Equipment Corporation, Maynard, MA, April 1997.

[11] Hawk, C.W., personal communication, University of Alabama in Huntsville, Propulsion Research Center, Huntsville, AL.

[12] Bryant, C.T., personal communication, Thiokol Corporation, Huntsville, AL.

[13] Huzel, D.K. and Huang, D.H., *Modern Engineering for Design of Liquid-Propellant Rocket Engines*, AIAA Progress in Astronautics, Vol. 147, 1992.

Appendix

Equation for measured C*:

$$C^* = \frac{\frac{\pi}{4}\left[\frac{\overline{D_0}^2 + \overline{D_1}^2}{2}\right]\left[h\left(\frac{1}{2}P_{0_1} + \sum_{i=2}^{i-1} P_{0_i} + \frac{1}{2}P_{0_i}\right)\right]}{\left(\overline{M}_{Fuel\ Tank} - \overline{M}_{Fuel\ Pump}\right) + \left[h\left(\frac{1}{2}\dot{m}_{LOX_1} + \sum_{i=2}^{i-1}\dot{m}_{LOX_i} + \frac{1}{2}\dot{m}_{LOX_i}\right)\right] + \left[h\left(\frac{1}{2}\dot{m}_{Nitrogen_1} + \sum_{i=1}^{N-1}\dot{m}_{Nitrogen_i} + \frac{1}{2}\dot{m}_{Nitrogen_N}\right)\right] + \left[h\left(\frac{1}{2}\dot{m}_{TEA_1} + \sum_{i=2}^{G-1}\dot{m}_{TEA_i} + \frac{1}{2}\dot{m}_{TEA_0}\right)\right]}$$